3D numerical modelling and laboratory study of flow field induced by a group of submerged vegetations

Ocean Engineering 312 (2024) 119038

Contents lists available at ScienceDirect

Ocean Engineering

journal homepage: www.elsevier.com/locate/oceaneng

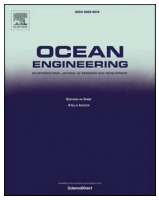

Research paper

3D numerical modelling and laboratory study of flow field induced by a group of submerged vegetations

Chukwuemeka Kingsley John [a], Jaan H. Pu [a,*], Yakun Guo [a], Mark Keating [b], Ebrahim Hamid Hussein Al-Qadami [c], Mohd Adib Mohammad Razi [c], Prashanth Reddy Hanmaiahgari [d]

[a] Faculty of Engineering and Digital Technologies, University of Bradford, Bradford, DB7 1DP, United Kingdom
[b] Flow Science, 3 Beverley Drive, Nottinghamshire, NG18 4QL, United Kingdom
[c] Faculty of Civil Engineering and Built Environment, Universiti Tun Hussien Onn, 86400, Parit Raja, Batu Pahat, Johor, Malaysia
[d] Department of Civil Engineering, Indian Institute of Technology Kharagpur, Kharagpur, 721302, India

ARTICLE INFO

Keywords:
Vegetation patch
Vegetation density
Computational fluid dynamics (CFD)
Acoustic Doppler velocimetry
Flow velocity
Flow turbulence

ABSTRACT

The three-dimensional (3D) numerical modelling in an open channel flow field of a group of submerged vegetations using computational fluid dynamics (CFD) platform of FLOW-3D HYDRO was performed in this study. A set of acoustic Doppler velocimetry (ADV) measurements have been conducted as benchmark to validate the numerical model. A quantitative comparison was performed on several hydrodynamic variables that impacted the vegetated open channel flow, such as flow depth, streamwise water velocity, turbulent intensity, and Reynolds shear stress. In the numerical analysis, the flow turbulence was treated using the RANS approach (within RNG k-ε); while the Volume Of Fluid (VOF) method was used to track the air-water interface. Structured meshes with hexahedral elements were used to discretize the channel geometry. In the findings, the numerical model reasonably reproduced the flow field and presented corresponding agreement with the experimental turbulent structures. This study showed that the differences in results between various analyses were all less than 10% and concludes that the presented numerical approach can be utilised as an efficient tool for simulations of the flow field within a vegetation patch (i.e. by using the simplified RANS approach).

1. Introduction

Vegetation-induced flow plays a significant role in shaping the hydrodynamic characteristics of aquatic environments. By the introduction of enhanced flow turbulence and vortices, the presence of submerged vegetation can significantly influence the flow field, especially in shallow flow environment (Wang and Wang, 2011). The induced turbulence can improve the water column's nutrient transport and mixing processes, which can have an impact on ecosystem health and water quality (Nepf, 2012; Xiang et al., 2019; Pu et al., 2022; Pu, 2022). Numerical models and laboratory studies are often used to study the complex interplay between submerged plants and water flow occurs on actual field cases. Laboratory experiments enable investigations of the flow processes induced by vegetation in controlled environment, while numerical methods, such as computational fluid dynamics (CFD), allow the prediction and analysis of the hydrodynamic and scouring effects by vegetation under various turbulence models, such as Direct Numerical Simulation (DNS), Large Eddy Simulation (LES) and Reynolds-Averaged Navier-Stokes (RANS) models (Corenblit et al., 2008; Murray et al., 2008; Camporeale et al., 2013; Koch and Pöschke, 2013; Gourgue et al., 2021; Dang et al., 2022).

The CFD models solve the Navier-Stokes equations and allow the incorporation of the effects of vegetation drag, its induced turbulence and vortex shedding. Through their simulations, the flow velocity, turbulence intensity, and Reynolds shear stress distribution around the vegetation can be analysed to provide valuable insights into hydrodynamic interactions between plants and surrounding flow field (Angelina and Jordanova, 2003; Pu et al., 2014; Kondziolka and Nepf, 2014; Pu, 2015; Solari et al., 2016; Maji et al., 2016; Pu et al., 2019; Smith et al., 2021; Ren et al., 2021). In theory, the CFD model employs finite or

* Corresponding author.
E-mail addresses: ifychuksdking@gmail.com (C.K. John), j.h.pu1@bradford.ac.uk (J.H. Pu), y.guo16@bradford.ac.uk (Y. Guo), markkeating4@gmail.com (M. Keating), ebrahim@uthm.edu.my (E.H.H. Al-Qadami), adib@uthm.edu.my (M.A. Mohammad Razi), hpr@civil.iitkgp.ac.in (P.R. Hanmaiahgari).

https://doi.org/10.1016/j.oceaneng.2024.119038
Received 16 June 2024; Received in revised form 31 July 2024; Accepted 17 August 2024
Available online 24 August 2024

meshless methods to solve non-linear differential equations of velocity, pressure and energy. Several studies have revealed that fluid dynamic behaviour is correlated to different essential process parameters such as reaction kinetics (Eslahpazir et al. 2011, 2019; Dang et al., 2022; Gupta et al., 2023a). CFD models allow generation of velocity fields in any specific geometry by inputting appropriate flow metrics prior to the simulation, including flow period, initial pressure and wall shear conditions (Taylor and Figueroa, 2009; Taylor and Steinman, 2010; Pourshahbaz et al., 2020).

On the other hand, the laboratory investigation can support numerical model by offering additional understanding of the flow dynamics caused by submerged vegetations. To examine their effects on the flow field in a controlled setting, researchers can adjust and modify a variety of parameters in the experiment, including plant density/amount, tested flow velocity and water depth. Particle image velocimetry (PIV) and Acoustic Doppler velocimetry (ADV) are two advance measurement techniques that can be used to provide reasonable flow structures and velocity measurements. Researchers can increase the accuracy and dependability on numerical models and deepen the understanding on intricate relationships between submerged vegetation and aquatic flows by validating the outcomes of numerical simulations with laboratory tests (Jones and Sandbach, 2020; Maji et al., 2020; Gupta et al., 2023b).

In the past, CFD was utilised to study simple single-phase systems, but more recently, it has been applied to a range of complex, multiphase processes (Bayon et al., 2016; Eslahpazir et al., 2019; Dang et al., 2022). There are several CFD simulation software in water and environmental management, where some examples include Openfoam, SimScale, Flowsquare, Ansys CFD, CFD Moule, Simcenter, and FLOW-3D (their full reviews can be found at Bayon et al., 2016; Pourshahbaz et al., 2020). The current study utilises the FLOW-3D HYDRO modelling software for its analysis. FLOW-3D HYDRO applies the dynamic boundary conditions at fluid-air surfaces, and it utilises proven numerical methods to track the location of surfaces, i.e. free surfaces are modelled with Volume of Fluid (VOF) technique. The FLOW-3D HYDRO software has been proven to be an accurate CFD software that focuses in solving transient, free-surface problems (Flow Science Inc, 2016; Choufu et al., 2019; Pourshahbaz et al., 2020; Kumar et al., 2024). Furthermore, FLOW-3D provides industry-specific solutions that are suited to the specific needs of several water and environmental engineering industries. Its specialised modules incorporate domain-specific features, allowing users to tailor unique problems and complexities of their respective professions and applications (Flow Science Inc, 2016).

The findings in this paper can help to give a better comprehension of the flow characteristics created by a group of vegetations within open channel. This study aimed to compare the acoustic Doppler velocimetry (ADV) experimental measurements and numerical results. To fulfil this aim, the study conducts a quantitative comparison between experimental and numerical data to evaluate the modelled turbulence parameters. In the proposed laboratory study, both the side and down-looking oriented probe were utilised in the ADV system (available at the Hydraulic Laboratory of University of Bradford). Side-looking ADV provides measurements across lateral extent, however it has a limitation to capture 5 cm of measurement near sidewall due to its required probe-to-measured point distance. On the other hand, the down-looking ADV can record point measurements except for 5 cm close to water surface. The combination of both ADVs can compensate one another, improve their weakness, and capture the maximum number of measured points. Even though ADV is having an intrusive nature in measurement, the detailed comparison of ADV and non-intrusive PIV has revealed the capability of ADV in open channel flow measurements (Ruonan et al., 2016). Ruonan et al. (2016) have found that apart from highly turbulent application, i.e. with turbulent kinetic flow energy located in the viscous range of power spectrum, the ADV has reproduced agreeing flow results with PIV measurement.

Tasar et al. (2023) evaluated experimental and numerical aspects on flow control using a 3-array submerged vane in a bent lab channel and discovered that the k-ε model is a practical and relatively accurate model for representing their tested condition. Tariq et al. (2022) studied 3D CFD modelling of flow characteristic under emerged and submerged vegetated flow conditions with circular-vegetation patches by big-scale varying densities, and they found the magnitude of turbulent structures were about 36% higher for submerged vegetation cases. Additionally, within the gap zone between vegetations, the increase in patch density considerably decreased the Reynolds stresses, turbulent kinetic energy, and turbulent intensities. Wang and Wang (2011) further proposed that the discrepancy between the simulation result and field observation can be as small as 15% for flow through submerged vegetation regions in a shallow lake using k-ε turbulence model. The results from this study provided another investigation into the k-ε-based turbulence model (i.e. RNG k-ε turbulence model). However, it used a more controllable approach in variation of vegetation stems amount. Instead of huge change in the vegetation density, it removed one stem to create free space for systematically studying the turbulence alteration. Through this investigation (using both experimental measurements and numerical modelling), the effect of limited space variation will be studied on its relative impact on the velocity and turbulence structure profiles as compared to fully packed vegetations.

In summary, this paper utilised the RNG k-ε turbulence numerical model to simulate the vegetation impact to experimental hydrodynamics parameters (such as turbulent intensity, and Reynold shear stress). The vertical distributions of streamwise velocity in different vegetation scenarios at various positions are analysed, and the impact of the vegetation on the flow distribution is studied. Through these analyses, this study contributes to the understanding of the internal flow turbulence and formed vortex that are crucial for flow-vegetation interaction investigation. Different vegetation amounts have been further investigated to identify their generated vortex impact towards flow turbulence structures, and hence quantifying the vortex generation mechanism in each case. Lastly, the combination use of numerical and experimental methods to study these phenomena is important as it can enhance the current understanding to complex vegetated zone influence on flow structures, which this shows the scientific contribution of this research.

2. Experimental and CFD methods

2.1. Experimental model

To find the reliability of the present simulations, experimental data were considered as benchmark solution. For this experimental study, a flume with length, width, and depth of 12 m, 0.5 m and 0.45 m respectively was used. Experiments were performed using a recently refurbished flume located at the Hydraulic Laboratory, University of Bradford. The flume operates through a circulating system, where the outlet discharge flows into a filtering tank then to a water pumping system to be re-directed back into the flume. The flume consists of glass walls and a smooth stainless-steel bed with group of vegetations screwed to the bed. A flat gate is located at the end of channel to control the flow depth in the flume. The flow discharge was regulated by a valve and measured by an electromagnetic flowmeter. Two parallel tracks (with trolleys) were attached on top of the flume, to hold and secure the ADV equipment. The submergence ratio for the vegetation in this study ranged from 0.47 to 0.72 and it was obtained by dividing the height of the submerged plant to the water depth. The submergence ratio is varying in the experiment, as the water depth was reduced from 21.5 cm to 13.8 cm from the up-to downstream of the vegetated area during the experiment. The submergence ratio is crucial for defining how much of vegetation is underwater, and how the vegetation influences the flow dynamics. The selected range of submergence ratio is within half-range of flow depth, but created large free-surface profile reduction, which can produce clear alteration to flow structures and clear test to velocity

profile.

The utilised vegetations was fixed to a rectangular plate with 2 cm base height. It contained 40 vegetations (i.e. 4 x 10) (Fig. 1). The diameter of the cylindrical vegetation was 1 cm. The vegetation plate was installed at 6 m away from the inlet tank to allow the settlement of inlet flow turbulence. The plate was fixed to the channel bed with eight screws, four at upstream and four at downstream. The screws did not interfere with flow of the water, as their leftover gaps were filled by silicon. The height of the vegetations was 10 cm (excluding 2 cm for the base) and they were spaced at 10 cm by 10 cm (Fig. 1a). Both the side-looking and down-looking probe ADVs, product of the Nortek Ltd (Vectrino ADV), were utilised in this experiment. Both ADVs are equipped with the four probe-receivers. Data from two duplicate z-direction probes can allow the minimising of measured data's noise when consider in the turbulence analysis (Blanckaert and Lemmin, 2006). The ADV is an intrusive device, however the measuring point is 5 cm away from the probe which can lessen its disturbance to flow measurement. Also, ADV is commonly regarded as a cost-effectiveness device compared to other more expensive methods of flow measurement. Some parameters (such as plant height, stem diameter, and density) were common design factors in field observations and literature on typical submerged vegetation (Fathi-Moghadam et al., 2011; Li and Xie, 2011; Tariq et al., 2022), which are also the design mechanisms of the utilised vegetation patch in this study. Five different points were selected and analysed in this study experimentally and numerically, and they include points A3, I3, J4, K3 and M4. Points A3 and M4 are points before and after the vegetation respectively while points I3, J4 and K3 are points within vegetation (refer to Fig. 1). Further, points I3 and K3 are in the vegetated row while point J4 is in the non-vegetated row.

Validation test was further analysed at points I3 and K3 with settings at Fig. 1b, where the vegetation at J3 location was removed. The numerical simulation and experimental results were produced at points I3 and K3 for comparison. This test was performed to investigate the impact of reduced vegetation numbers (or increased adjacent vegetation spacing) in the vegetated flow.

2.2. CFD analysis

The utilised FLOW-3D HYDRO model uses the Cartesian staggered grid to solve the Reynolds' Average Navier-Stokes (RANS) equations. The model uses the finite volume method (FVM) to spatially discretize the conservation equations, while the Fraction Area/Volume Obstacle Representation (FAVOR) approach is employed to track the fluid-solid interface. As suggested by Rodi (1993) and Zaffar and Hassan (2023), the following equations can be utilised to represent flow conditions:

$$\frac{\partial}{\partial x_j}\left(\rho u_j\right) = 0 \tag{1}$$

$$\frac{\partial}{\partial x_j}\left(\rho u_i u_j\right) = -\frac{\partial p}{\partial x_j}\partial_{ij} + \frac{\partial}{\partial x_j}\mu\left(\frac{\partial u_i}{\partial x_j} + \frac{\partial u_j}{\partial x_i}\right) + \frac{\partial}{\partial x_j}\left(-\rho u_i u_j\right) \tag{2}$$

The momentum equation for incompressible flow considered in this study is:

$$\rho\left(\frac{\partial u}{\partial t} + u\nabla u\right) = -\nabla\rho + \mu\nabla^2 u + \rho g \tag{3}$$

The pressure and fluid density in Equations (1)–(3) are represented by p and ρ, respectively. ∇, g, and ∂t are the convective derivative, acceleration due to gravity and change in time respectively while the viscosity proportionality constants and velocity of the fluid are denoted by μ and u respectively. The CFD model employs Reynolds averaged Navier Stokes equations (RANS) to represent flow turbulence. Turbulence models solve for closure by averaging the Reynolds stress terms in the Navier-Stokes equation and adding variables to turbulent and dissipation equations (Zaffar and Hassan, 2023). Three different mesh densities were used to conduct the sensitivity analysis which include 1, 592,750 (low), 2,496,900 (intermediate) and 3,260,000 cells (high resolution). The results from the sensitivity analysis showed similar patterns for three solutions. In Fig. 2, the finest mesh resolutions gave the most accurate results but with highest computational cost, while the coarse resolution presented the least accurate results and shortest computational time. The intermediate mesh resolution showed the most optimum results with regards to accuracy versus computational cost and was thus selected for use in the current CFD analysis. To save computational effort, the coarse mesh was used for the entire volume of the flume except for the positions of vegetation patch, where intermediate mesh was used. This was done to provide detail information of events occurring within the vegetated zone.

2.3. Turbulence model

In DNS model, the eddies can be numerically resolved down to its lowest scale, but this approach is highly demanding computationally for representing any engineering real-world application (Bayon et al.,

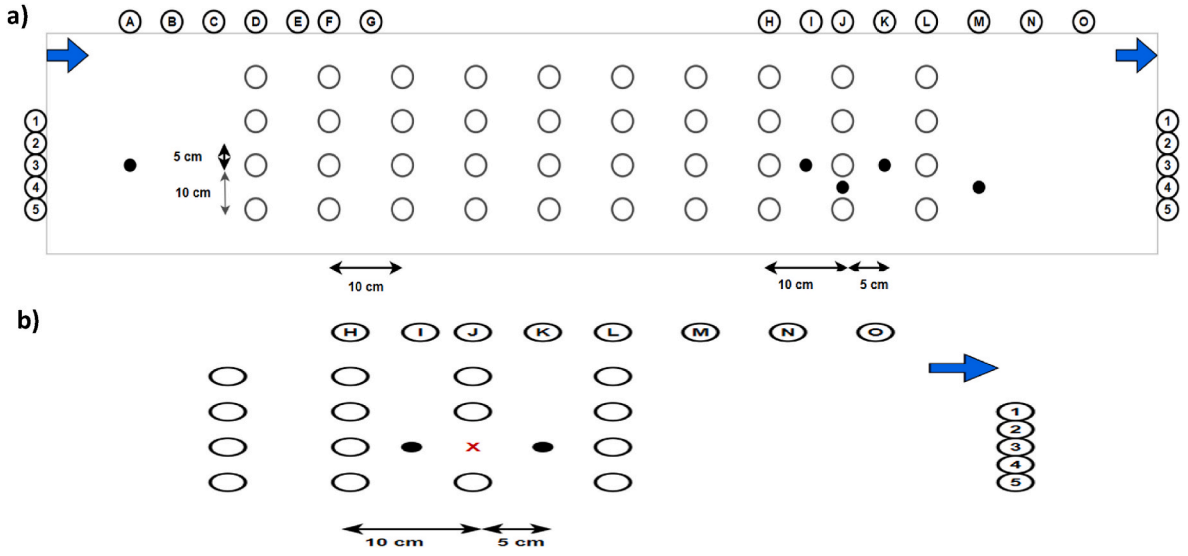

Fig. 1. Views of the vegetations; (a) main tests; and (b) validation tests. (The black dot denotes experimental measured and numerical simulated points, while the red x denotes points the vegetation location that was taken off).

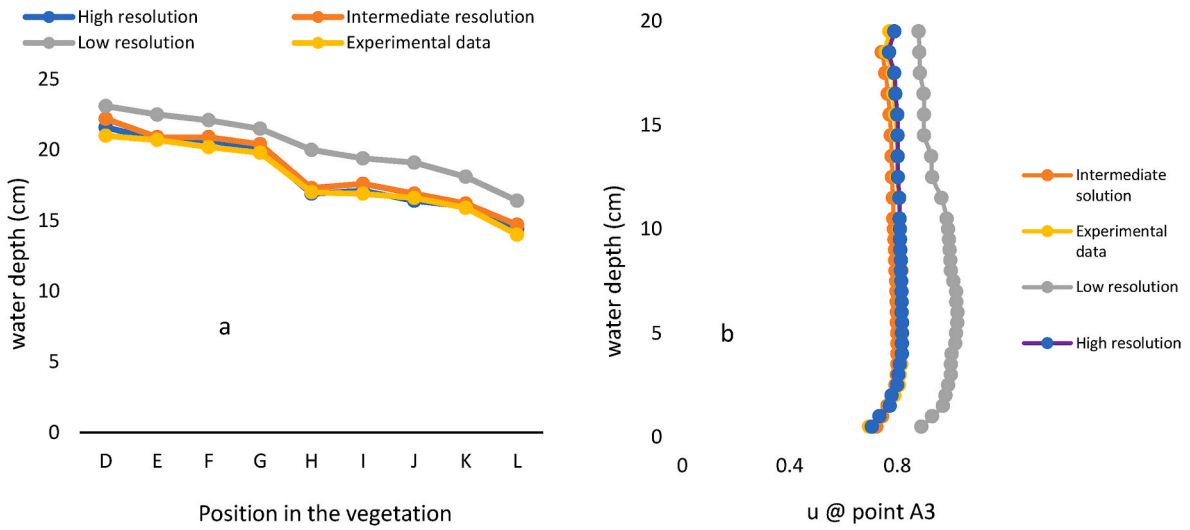

Fig. 2. Mesh sensitivity analysis: (a) water depth; (b) streamwise velocity at point A (Fig. 1).

2016). Several studies such as Borue et al. (1995); Nagosa (1999); Prosperetti and Tryggvason (2007) have applied DNS to simulate multiphase flow, however, their models are in-realistically expensive. The LES techniques provide accurate multiphase flow simulations at a reasonably reduced computational cost compared to DNS, however still expensive for most engineering applications (Spalart, 2000; Bayon et al., 2016). One of the most widely utilised practical approach in engineering applications is the Reynolds Averaged Navier-Stokes (RANS) model (Pope, 2000; Bayon et al., 2016; *FLOW-3D® Version 2023R1, 2023*).

In the present study, the chosen turbulence model was based on RNG k-ε method (Flow Science Inc, 2016). The RNG k-ε turbulence model was proposed by Yakhot et al. (1992), while other standard two-equation k-ε models have also been intensely studied (Kasiteropoulou et al., 2017; Tasar et al., 2023). The RNG k-ε turbulence model has an additional term in its ε equation compared to standard k-ε model. This additional term improved the accuracy for swirling and quickly strained flows to give better result convergency as suggested by the numerical investigations of Carvalho et al. (2008); Bayon et al. (2016); Daneshfaraz et al. (2020); Ghaderi and Abbasi (2019); and Ghaderi et al. (2020a, b).

2.4. Boundary conditions (BCs)

Fig. 3 presents the boundary conditions for test around the key vegetated area. The BCs for Y_{max}, Y_{min} and Z_{min} are Wall (W), while the BC for Z_{max} is governed by the atmospheric pressure condition (P) (Fig. 3).

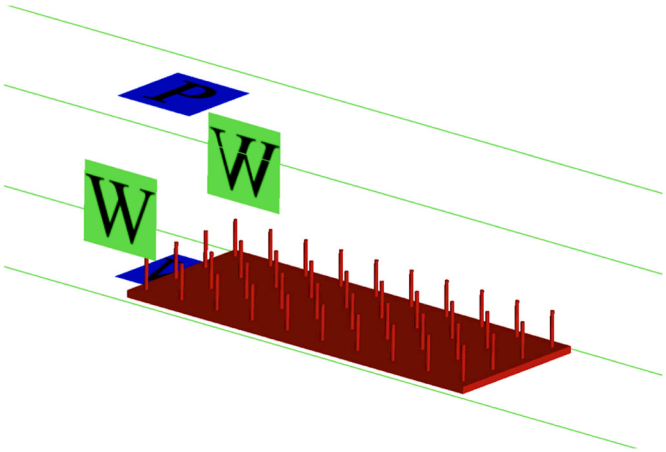

Fig. 3. Boundary conditions for the vegetated zone.

The inlet and outlet BCs are flow rate (Q) and P respectively. A solid block was used for the floor that prescribed by the surface and bottom roughness, and is calculated using a minimum roughness height input of 0.5 mm. The flume was set at a slope of 0.3375%. The flow rate (Q) was set at 0.0775 m^3/s and the mean flow velocity at undisturbed region was 0.76 m/s, while the flow elevations at the inlet were 0.215 m. These values of channel slope, discharge, velocity and flow elevations were obtained from the laboratory test.

2.5. Computational grid

Unstructured meshes permit selective refinement of areas where large gradients of flow variables are anticipated. Their arbitrary topology makes them fit better into complex geometries as well as show fewer closure issues. However, in comparison, use of a structured mesh approach tends to solve quicker for a similar mesh resolution, as well as being more straight forward to apply (Biswas and Strawn, 1998; Kim and Boysan, 1999; Bayon et al., 2016). Moreover, structured mesh tends to develop a more regular access to memory, thereby reducing the latency of simulation (Keyes et al., 2000; Bayon et al., 2016; Quaresma and Pinheiro, 2021). Consequently, a structured rectangular hexahedral mesh was utilised as it is more suited to the timely objective in this study. The employed computational domains are split into a structured mesh grid of variable-sized hexahedral cells utilising Cartesian coordinates. The computational grid is characterised independently by the geometry and afterwards assigned into grid system (Quaresma and Pinheiro, 2021; Flow Science Inc, 2022; *FLOW-3D® Version 2023R1, 2023*).

A stability criterion, i.e. Courant criteria, was adopted to compute the allowable time-step size (Pu et al., 2012; Ghaderi et al., 2020a, 2021). The computation was performed using a personal computer that has an eight core CPU (Intel Core i7-11800H @ 4.6 GHz and 16 GB RAM). The solid object representing the submerged vegetation was generated using AutoCAD 2020 (AutoDesk, San Rafael, CA, USA) based on dimensions of the physical laboratory model and it was imported into FLOW-3D HYDRO as a stereolithography (stl) file (refer to Fig. 4).

3. Results and discussion

The comparison of water depth between the measurements and CFD simulation is presented in Fig. 5. The simulated water depth was having less than 4% of discrepancy when benchmarked by measurements.

Observation showed that there was a sudden reduction in the water

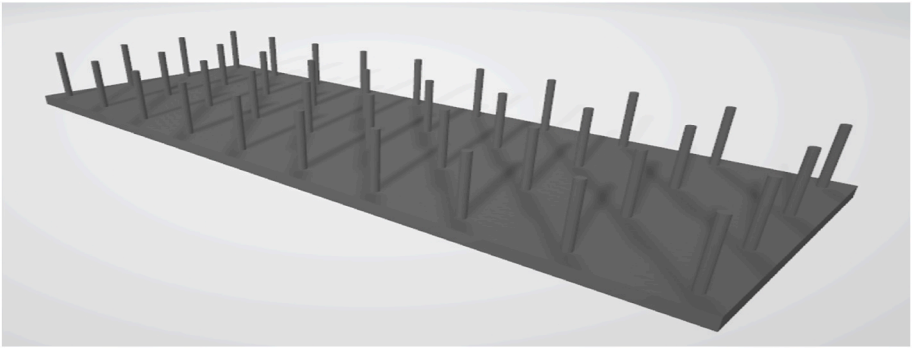

Fig. 4. Submerged vegetation imported into FLOW-3D HYDRO as a stl file.

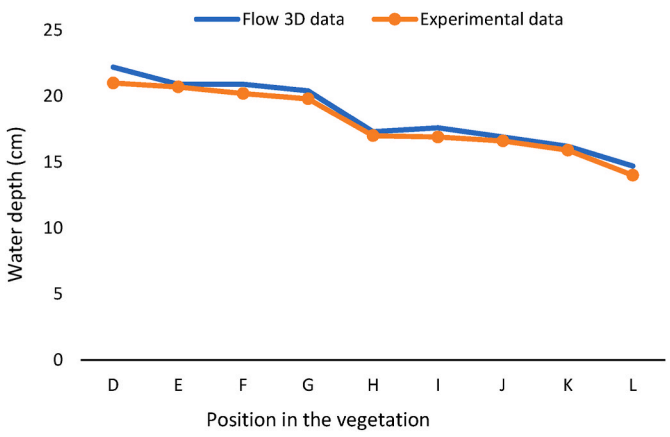

Fig. 5. Comparison of the water depth from the experimental data and FLOW-3D HYDRO (Points D to L are shown in Fig. 1).

depth from the upstream to the downstream at position H. Positions G and H were 55 cm apart (refer to Fig. 1), hence the drop of flow depth from upstream (G) to downstream (H) was un-avoidable after flow passing across a lengthy portion of vegetation zone. The water depth at the start and end of vegetation zone are 21.5 cm and 14 cm respectively. Five different measured points were selected and further analysed in this study, and they include points A3, I3, J4, K3 and M4 (refer to Fig. 1 for the point locations).

3.1. Streamwise velocity

Fig. 6 presents the comparison of the streamwise velocity (u) from the CFD modelling and laboratory data. The comparison points of A3, I3, J4, K3 and M4 have been used in Fig. 6 (and the following Figs. 8–10), as I3, J4, and K3 were located within the vegetation zone, while A3 and M4 were situated before and after that zone, respectively. These comparisons can reveal the ability of numerical model to consistently simulate of the vortex-induce flow within the vegetation, the undisturbed flow prior to the vegetation patch and flow recovery after the vegetated zone, to fully validate the presented model. Results showed some discrepancies between both data, where majority of the differences were observed in the middle section of plots. Those discrepancies in the computed plot (as compared to experimental data) have been caused by the vegetation-stem created turbulence and eddies in the area covered by the height of vegetation. The presence of the vegetation as an obstruction causes a mixture of strong and weak eddies to be generated, which has not been sufficiently represented by the RNG k-ε turbulence model.

For comparison and benchmarking purposes, the u profile at point A3 (before the vegetation patch) has been simulated, which both measured and computed results presented agreeing open channel flow profile. This shows the model's accuracy in relatively less vortex-impacted area. Further observation showed positive values of u were observed throughout the profile at points I3, J4 and K3, while mixture of positive to negative profile were found at point M4. The u values continuously reduced away from the bed to water surface at I3 and K3 while multiple changes experienced at J4. The profile differences are a result of their relative positions within the vegetation patch. The eddies generated at points between vegetations (i.e., I3 and K3) caused continuous reduction in the u value from near bed to water surface (see Fig. 6). On the other hand, at M4, u reduced from positive to negative

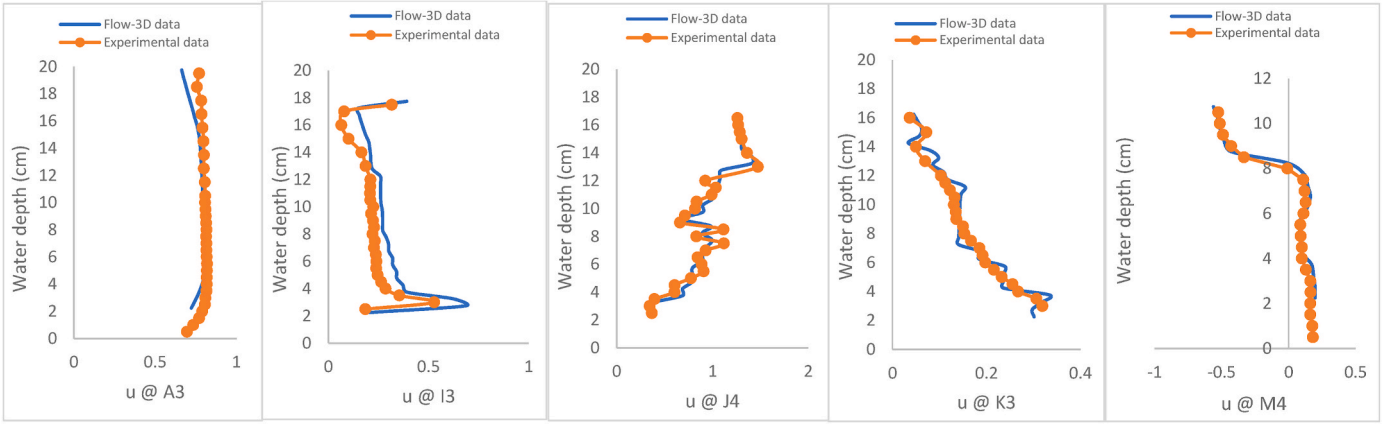

Fig. 6. Comparison of the streamwise velocity (m/s) from experimental and FLOW-3D HYDRO data for five points (U signifies streamwise velocity). Points A3 and M4 are points before and after the vegetation plate respectively while points I3 and K3 are in the vegetated row while point J4 is in the non-vegetated row.

value at 8 cm of water depth (Fig. 6) due to the strong vortices impact at the top of vegetation.

The experimental results of the streamwise velocity in this study agree with studies from Huai et al. (2009), Pu et al. (2019) and Vijayasree et al. (2020). Huai et al. (2009) and Pu et al. (2019) which reported that higher velocity variations was observed in the point between adjacent vegetations. Agreed with Vijayasree et al. (2020), in this study, the horseshoe vortices at the upstream vegetation immediately bifurcate through sideways and transfer to wake vortices at the downstream, and it sustains for a longer distance before dissipation and therefore impacts the points between adjacent vegetations. In the observation, the vortex-induced velocity profile has been captured with reasonable discrepancy by the numerical model, which proved the capability of the employed CFD model and its utilised practical turbulence modelling approach. Fig. 7 depicts the schematic diagram for the vortex occurring space in Tests 1 and 2. The variable vegetation spacing sizes are responsible for the local difference in velocities inside the vegetation patch in different tests. In Test 1, the presence of plant stems limited the creation of turbulent vortex, while this phenomenon was stronger in more open space in Test 2 resulting the change in velocity.

The root-mean-square error for modelled streamwise velocity (in reference to the measured data) at points A3, I3, J4, K3 and M4 has been observed to be 2.0%, 6.3%, 7.2%, 3.5% and 5.5% respectively. The standard deviation for those points is 3.9%, 9.5%, 28.3%, 8.3% and 28.7% respectively. The standard deviation data were generated to highlight the uncertainties for those modelled datasets. The results of the present numerical simulations show that the velocity profile distributions reflect the flow and turbulent structures of those from the experimental measurements without significant discrepancy.

3.2. Turbulent intensity

Fig. 8 presents the comparison of the turbulent intensity from experimental and computed data for five investigated points. Positive values for turbulent intensity were observed in all the five points. At point A3, the turbulent intensity reduced away from the bed before maintaining constant till almost the water surface, due to absent of vegetation obstruction. Continuous reduction in turbulent intensity occurred away from bed to water surface in K3, while the turbulent intensity reduced away from the bed till 7 cm at M4 (Fig. 8). The root-mean-square error for simulated turbulent intensity (as benchmarked by the experimental data) for points A3, I3, J4, K3 and M4 are 1.2%, 5.6%, 4.2%, 2.2% and 1.2% respectively. Furthermore, the comparison of the turbulent intensity profile of the experimental measurements and numerical simulations showed a corresponding profile distribution, which indicate the reasonable accuracy of presented simulation.

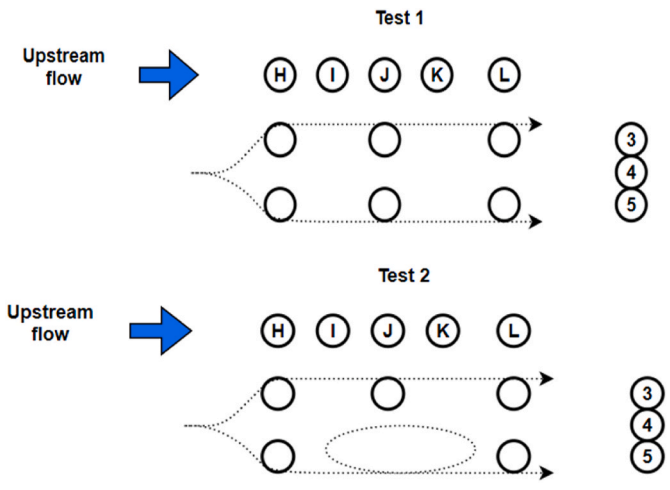

Fig. 7. Schematic diagram for turbulent vortex development. The dotted circles in Test 2 denote the vortex generation area while the solid circles denote the vegetation stems.

3.3. Reynold's shear stress

Fig. 9 shows the comparison of the Reynolds shear stress between the measured and simulated data at different points. Results showed that the Reynolds shear stress profiles are close to zero at the measured points within the vegetations (i.e., at points I3, J4 and K3). The Reynolds shear stress values at A3 increased to positive throughout the water depth, while mix of increment and decrement was seen at M4. Despite the continuous increase and decrease in values at M4, the Reynolds shear stress profile was wholly in negative region. Benchmarked by laboratory data, the modelled data's root mean square error for Reynold shear stress at points A3, I3, J4, K3 and M4 are 1.2%, 0.2%, 3.7%, 0.2% and 2.8% respectively, thus indicating reasonable agreement with measurements.

Some Reynolds shear stress plots in Fig. 9 were observed to be in negative region, especially at I3, J4, K3, and M4. It showed intricate interactions within complex vortices within and after vegetated zone. Several reasons, including flow separation and reattachment, turbulence formation, shear layer dynamics, and intrinsic flow variability, were key in causing this negative profile, as also suggested in other similar studies (such as Maji et al., 2017; Xuecheng et al., 2020; Pasha et al., 2023; John et al., 2023). This negative profile was not observed in turbulent intensity profiles, as in comparison, Reynolds stress involves multiple dimensional fluctuating velocities (u' and v') that can present opposing signs in areas of high vortex recirculation.

The analysis of both the modelled and experimental results produced physically consistent profiles for the selected five points, as seen in Figs. 5, 6, 8 and 9, which proved the ability of the numerical model to adequately reproduce the complex flow field of a group of submerged vegetations in an open channel flow. The agreement in the comparison also indicates that the selected RNG k-ε turbulence model can be used to reasonably represent the flow field of a group of submerged vegetation hydrodynamics. The difference between the experimental measurements and the CFD simulation was kept less than 10% in all modelled data. However, it is imperative to note that the right boundary conditions and multi-physics tools are needed to be used, which show the cruciality of the step-by-step tests from sensitivity to velocity profile and turbulent structure analyses presented in this study.

3.4. Vegetation spacing tests

In Fig. 10, turbulent characteristics (including streamwise velocity, turbulence intensity, and Reynolds stress) were presented for points I3 and K3 after the removal of one vegetation at point J3. Using the same boundary conditions with the results generated in Figs. 6, 8 and 9, the computed profiles showed similar trend with the experimental data. The u profile for point K3 showed continuous reduction away from the bed; while for point I3, the u value reduced away from the bed till 10 cm, which is corresponding to the height of vegetation (Fig. 10a). The u profile for the computed results at points I3 and K3 are close to the laboratory data with the respective root mean square error of 2.54% and 2.2%. Similar to the u profile results, the turbulence intensity and the Reynold shear stress results for numerical and experimental data are close (Fig. 10b and c). The computed root mean square error for turbulence intensity and Reynold shear stress benchmarked by laboratory data for point I3 are 6.9% and 0.3% respectively, whereas they are 7.6% and 0.74% respectively for point K3. The root mean square error for all results are adequate (less than 8%). The results obtained in Fig. 10 are different from those in Figs. 6, 8 and 9 due to larger open space between adjacent vegetations to create different vegetation spacing. Also, due to the open spaces created by the removal of vegetation at point J3, the turbulence intensity reduced from I3 to K3 between the water depth of 2 cm–10 cm (Fig. 10b).

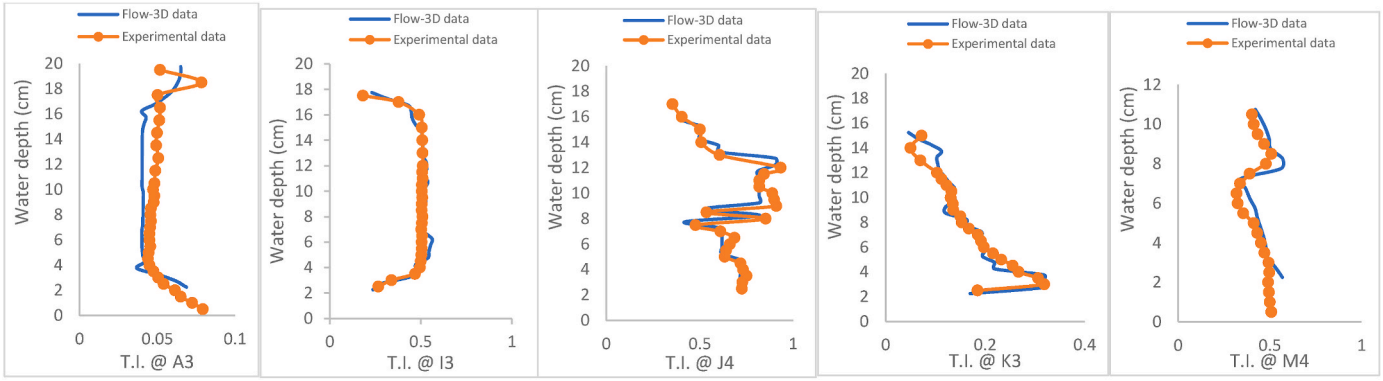

Fig. 8. Comparison of the turbulent intensity (unitless) from experimental and FLOW-3D HYDRO data for five points (T.I. signifies Turbulence Intensity). Points A3 and M4 are points before and after the vegetation plate respectively while points I3 and K3 are in the vegetated row while point J4 is in the non-vegetated row.

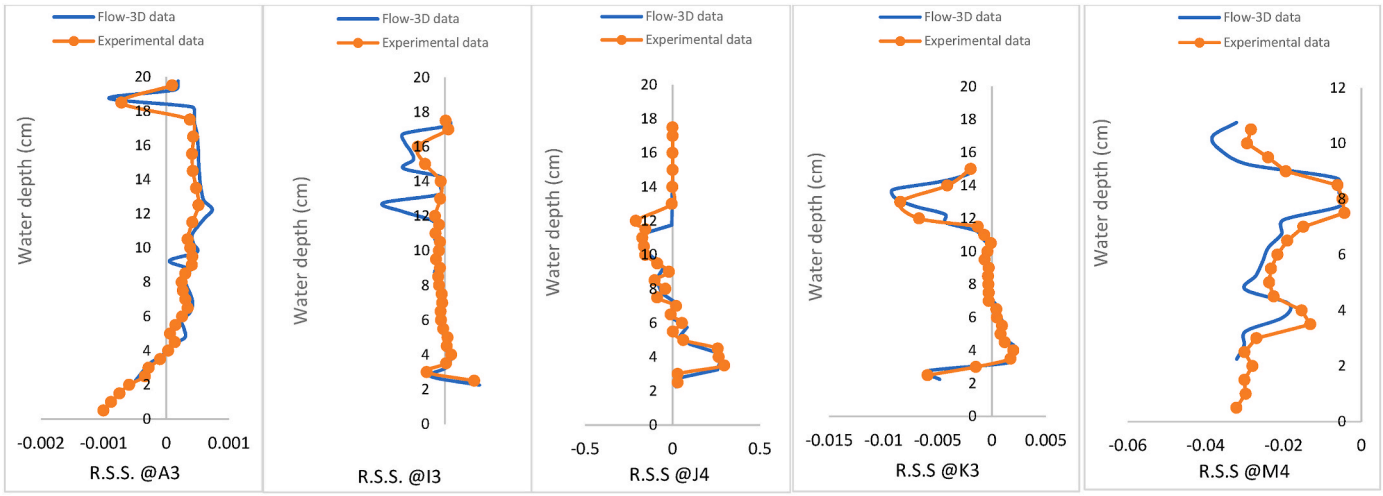

Fig. 9. Comparison of the Reynold shear stress (unitless) from experimental and FLOW-3D HYDRO data for five points (R.S.S. signifies Reynold shear stress). Points A3 and M4 are points before and after the vegetation plate respectively while points I3 and K3 are in the vegetated row while point J4 is in the non-vegetated row.

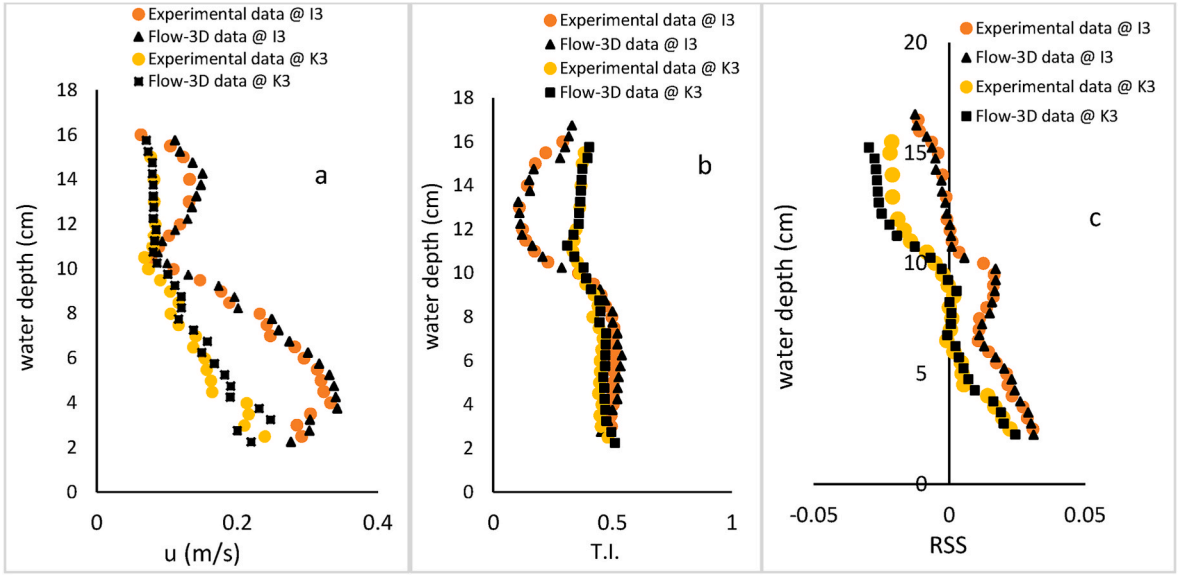

Fig. 10. Validation test for a) u, b) turbulence intensity, and c) Reynolds shear stress.

3.5. Limitation of the study

Input data accuracy, and modelling assumptions (i.e. turbulence modelling method) are the primary sources of uncertainty in this study's numerical simulations. Inaccuracies in initial and boundary conditions, geometric representations, and numerical techniques can introduce calculative errors and variances in simulation outcomes. Furthermore, some flow complexities may not be captured by simplified RNG k-ε turbulence model. When compared with experiment, these uncertainties may affect how accurate the anticipated flow fields are predicted. In this study, the numerical validation (benchmarked by experimental measurements) has been used to ensure such errors are within acceptable range.

Also, the numerical model is scalable for more complex real-world channel geometries and vegetation distributions due to its utilised practical and less computationally demanding turbulence model. The requirement for increasingly demanding input data and model assumptions for correct depiction of complex real-world geometries and varied vegetation patterns, as well as resulted rising processing demands and possible numerical stability problems, are major obstacles to scaling up simulations. To tackle these obstacles and ensure accurate results in more complicated settings, more validation (i.e. through real-world application) is needed.

4. Conclusion

This study investigated a numerical model created in FLOW-3D numerical environment to simulate the open channel flow velocity and turbulent structures with submerged rigid vegetations. The utilised vegetation patch has equal spacing of 10 cm laterally and longitudinally from each other. A further test with removing a single vegetation has also been conducted to study spacing variation impact to flow velocity and turbulence structures. The simulation results were further compared to the conducted experiments which was obtained using both side and down-looking ADVs.

It was observed that several hydrodynamic parameters were significantly altered by the present of submerged vegetation patch, such as flow depths, streamwise water velocity, turbulent intensity and Reynolds shear stress. The analysis further revealed that numerical model represented the measured flow with more discrepancy in mid-flow area compared to the bottom and water surface regions. This is due to the heavy vortex in mid-flow region, as compared to water surface and near bed regions, that presented escalated difficulty for numerical model to represent. The points selected for comparison included point before the vegetation patch (i.e., point A3), point between adjacent vegetations (i.e., point J4), points between vegetations (i.e., points I3 and K3) and point after the vegetation patch (i.e., point M4). These points were chosen to allow effective numerical validation, as they show variations in the turbulence structure as flow travels from up-to downstream. All point comparison results showed the root-mean-square error of lesser than 10%, which indicated reasonable agreement between the modelled and experimental data. However, the discrepancy in numerical simulation with measurements, especially in the mid-flow region within vegetated zone, showed caution to the utilised RNG k-ε approach. Since the RNG k-ε approach approximates flow turbulence structures from numerically estimated k and ε terms, it has been proven to be less capable to represent heavy vortex zone within the studied vegetated flows. However, it has shown reasonable simulation to the recovery and less vortex impact zones, which illustrates its potential use due to the practical simulation efficiency that it presents. To evaluate and improve the present numerical modelling approach, its applicability to real-world flow scenarios should also be further studied.

Data availability statement

The data of this study are available from the corresponding author upon reasonable request.

Funding statement

No funding has been obtained for conducting this study.

CRediT authorship contribution statement

Chukwuemeka Kingsley John: Writing – original draft, Methodology, Investigation, Formal analysis, Conceptualization. **Jaan H. Pu:** Writing – review & editing, Writing – original draft, Supervision, Resources, Project administration, Methodology, Conceptualization. **Yakun Guo:** Writing – review & editing, Supervision, Methodology. **Mark Keating:** Writing – review & editing, Methodology. **Ebrahim Hamid Hussein Al-Qadami:** Writing – review & editing, Methodology. **Mohd Adib Mohammad Razi:** Writing – review & editing, Methodology. **Prashanth Reddy Hanmaiahgari:** Writing – review & editing, Methodology.

Declaration of competing interest

The authors declare that they have no conflict of interest.

References

Angelina, A., Jordanova, C.S.J., 2003. Experimental study of bed load transport through emergent vegetation. J. Hydraulic Eng. ASCE 129 (6), 474–478, 2003.

AUTOCAD, 2020. https://www.autodesk.com/support/technical/article/caas/sfdcarticles/sfdcarticles/System-requirements-for-AutoCAD-2020-including-Specialized-Toolsets.html.

Bayon, A., Valero, D., García-Bartual, R., Valles-Morana, F.J., Lopez-Jimenez, P.A., 2016. Performance assessment of OpenFOAM and FLOW-3D in the numerical modeling of a low Reynolds number hydraulic jump. Environ. Model. Software 80 (2016), 322–335.

Biswas, R., Strawn, R.C., 1998. Tetrahedral and hexahedral mesh adaptation for CFD problems. Elsevier Appllied Numerical Mathematics 26 (1), 135–151.

Blanckaert, K., Lemmin, U., 2006. Means of noise reduction in acoustic turbulence measurement. J. Hydraul. Res. 44 (1), 3–17.

Borue, V., Orszag, S., Staroslesky, I., 1995. Interaction of surface waves with turbulence: direct numerical simulations of turbulent open channel flow. J. Fluid Mech. 286, 1–23.

Carvalho, R., Lemos, C., Ramos, C., 2008. Numerical computation of the flow in hydraulic jump stilling basins. J. Hydraul. Res. 46 (6), 739–752.

Choufu, L., Abbasi, S., Pourshahbaz, H., Taghvaei, P., Tfwala, S., 2019. Investigation of flow, erosion, and sedimentation pattern around varied groynes under different hydraulic and geometric conditions: a numerical study. Water 11, 235, 2019.

Camporeale, C., Perucca, E., Ridolf, L., et al., 2013. Modeling the interactions between river morphodynamics and riparian vegetation. Rev. Geophys. 51, 379–414.

Corenblit, D., Gurnell, A.M., Steiger, J., et al., 2008. Reciprocal adjustments between landforms and living organisms: extended geomorphic evolutionary insights. Catena 73, 261–273.

Daneshfaraz, R., Ghaderi, A., Akhtari, A., Di-Francesco, S., 2020. On the effect of block roughness in ogee spillway with flip buckets. Fluid 5, 182, 2020.

Dang, X., Huai, W., Zhu, Z., 2022. Numerical simulation of vegetation evolution in compound channels. Environ. Sci. Pollut. Control Ser. 30, 1595–1610.

Eslahpazir, M., Krull, R., Moo-Young, M., 2011. Engineering Fundamentals of Biotechnology, Comprehensive Biotechnology, second ed. Elsevier. eBook ISBN: 9780080885049.

Eslahpazir, M., Kruhne, U., Moo-Young, M., 2019. Engineering Perspectives in Biotechnology, Comprehensive Biotechnology, second ed. Elsevier. eBook ISBN: 9780080885049.

Fathi-Moghadam, M., Kashefipour, M., Ebrahimi, N., Emamgholizadeh, S., 2011. Physical and numerical modeling of submerged vegetation roughness in rivers and flood plains. J. Hydrol. Eng. 16 (11) https://doi.org/10.1061/(ASCE)HE.1943-5584.0000381.

FLOW-3D® Version 2023R1, 2023. Santa Fe, NM: Flow Science. Inc. [Computer software] https://www.flow3d.com.See. (Accessed 30 August 2023). https://www.flow3d.com/resources/bibliography/how-to-reference-flow-3d-products/

Flow Science Inc, 2016. Flow-3D V 11.2 User's Manual. Flow Science Inc., Santa Fe, NM, USA, 2016.

Flow Science Inc, 2022. TruVOF and Free Surface Modelling. Why FLOW-3D? Best CFD Software for Free Surface Flows (flow3d.Com). (Accessed 17 September 2022).
Ghaderi, A., Abbasi, S., 2019. CFD simulation of local scouring around airfoil-shaped bridge pier with and without collar. Sadhana 44, 216, 2019.
Ghaderi, A., Daneshfaraz, R., Dasineh, M., Di-Francesco, S., 2020a. Energy dissipation and hydraulics of flow over trapezoidal-triangular labyrinth weirs. Water 2020 (12), 1992.
Ghaderi, A., Dasineh, M., Aristodemo, F., Ghahramanzadeh, A., 2020b. Characteristics of free and submerged hydraulic jumps over different macroroghness. J. Hydroinf. 2020 (22), 1554–1572.
Ghaderi, A., Dasineh, M., Aristodemo, F., Arico, C., 2021. Numerical simulations of the flow field of a submerged hydraulic jump over triangular macroroughness. Water 2021 (13), 674–698.
Gourgue, O., Belzen, J., Schwarz, C., et al., 2021. A convolution method to assess subgrid-scale interactions between flow and patchy vegetation in biogeomorphic models. J. Adv. Model Earth Sys. https://doi.org/10.1029/2020ms002116.
Gupta, L.K., Pandey, M., Anand Raj, P., 2023a. Numerical simulation of local scour around the pier with and without airfoil collar (AFC) using FLOW-3D. Environ. Fluid Mech. 1–19. https://doi.org/10.1007/s10652-023-09876-1.
Gupta, L.K., Pandey, M., Raj, P.A., 2023b. Numerical modelling of scour and erosion processes around spur dike. CLEAN–Soil, Air, Water, 2300135.
Huai, W.X., Zeng, Y.H., Xu, Z.G., Yang, Z.H., 2009. Three-layer model for vertical velocity distribution in open channel flow with submerged rigid vegetation. Adv. Water Resour. 32 (2009), 487–492.
John, C.K., Pu, J.H., Guo, Y., Hanmaiahgari, P.R., Pandey, M., 2023. Flow turbulence presented by different vegetation spacing sizes within a submerged vegetation patch. J. Hydrodyn. 35 (6), 1131–1145.
Jones, M.T., Sandbach, S.D., 2020. Laboratory study of flow field induced by a group of submerged vegetations: insights and validation of numerical models. Water Res. 45 (2), 215–227.
Kasiteropoulou, D., Liakopoulos, A., Michalolias, N., Keramaris, E., 2017. Numerical modelling and analysis of turbulent flow in an open channel with submerged vegetation. Environmental Processes 4, 47–61.
Keyes, D., Ecer, A., Satofuka, N., Fox, P., Periaux, J., 2000. Parallel Computational Fluid Dynamics' 99: towards Teraflops, Optimization and Novel Formulations. Elsevier.
Kim, S.-E., Boysan, F., 1999. Application of CFD to environmental flows. Elsevier J. Wind Eng. Industrial Aerodynamics 81 (1), 145–158.
Koch, W., Pöschke, F., 2013. Vegetation in river systems: effects on hydraulic properties. River Res. Appl. 29 (6), 723–739.
Kondziolka, J.M., Nepf, H.M., 2014. Vegetation wakes and wake interaction shaping aquatic landscape evolution. Limnol. Oceanogr. Fluid. Environ. 4, 106–119.
Kumar, B., Pandey, M., Ahmad, Z., 2024. Flow field and sediment passing capacity of type-a piano key weirs. Int. J. Sediment Res. https://doi.org/10.1016/j.ijsrc.2023.100280.
Li, C.W., Xie, J.F., 2011. Numerical modelling of free surface flow over submerged and highly flexible vegetation. Adv. Water Resour. 34 (4), 468–477.
Maji, S., Pal, D., Hanmaiahgari, P., Pu, J.H., 2016. Phenomenological features of turbulent hydrodynamics in sparsely vegetated open channel flow. J. Appl. Fluid Mech. 9 (6), 2865–2875.
Maji, S., Pal, D., Hanmaiahgari, P.R., 2017. Hydrodynamics and turbulence in emergent and sparsely vegetated open channel flow. Environ. Fluid Mech. 17, 853–877, 2017. https://doi-org.brad.idm.oclc.org/10.1007/s10652-017-9531-2.
Maji, S., Hanmaiahgari, P.R., Balachandar, R., Pu, J.H., Ricardo, A.M., Ferreira, R.M.L., 2020. A review on hydrodynamics of free surface flows in emergent vegetated channels. Water (MDPI) 12 (4), 1–17. Article No. 1218.
Murray, A.B., Knaapen, M.A.F., Tal, M., et al., 2008. Biomorphodynamics: physical-biological feedbacks that shape landscapes. Water Resour. Res. 44, W11301.
Nagosa, R., 1999. Direct numerical simulation of vortex structures and turbulence scalar transfer across a free surface in a fully developed turbulence. Phys. Fluid. 11, 1581–1595.
Nepf, H.M., 2012. Flow and transport in regions with aquatic vegetation. Annu. Rev. Fluid Mech. 44 (1), 123–142.
Pasha, G.A., Ghumman, A.R., Naseer, M.J., 2023. Flow characteristics in a two-stage vegetated compound trapezoidal channel. Iran J Sci Technol Trans Civ Eng 47, 505–517, 2023. https://doi-org.brad.idm.oclc.org/10.1007/s40996-022-00904-y.
Pope, S.B., 2000. Turbulent Flows. Cambridge university press.
Pourshahbaz, H., Abbasi, S., Pandey, M., Pu, J.H., Taghvaei, P., Tofangdar, N., 2020. Morphology and hydrodynamics numerical simulation around groynes. ISH. J. Hydraul. Eng. 2020, 1–9.
Prosperetti, A., Tryggvason, G., 2007. Computational Methods for Multiphase Flow. Cambridge University Press.
Pu, J.H., Cheng, N.S., Tan, S.K., Shao, S., 2012. Source term treatment of SWEs using surface gradient upwind method. J. Hydraul. Res. 50 (2), 145–153.
Pu, J.H., 2015. Turbulence modelling of shallow water flows using Kolmogorov approach. Comput. Fluid 115, 66–74.
Pu, J.H., Pandey, M., Li, J., Satyanaga, A., Kundu, S., Hanmaiahgari, P.R., 2022. Editorial: urban fluvial and hydro-environment system. Front. Environ. Sci. 10, 1–3. Article No. 1075282.
Pu, J.H., 2022. Editorial: environmental hydraulics, turbulence and sediment transport. Fluids (MDPI) 7 (48), 1–2.
Pu, J.H., Hussain, A., Guo, Y., Vardakastanis, N., Hanmaiahgari, P.R., Lam, D., 2019. Submerged flexible vegetation impact toward open channel flow velocity distribution: an analytical modelling study on drag and friction. Water Sci. Eng. 12 (2), 121–128.
Pu, J.H., Hussain, K., Shao, S., Huang, Y., 2014. Shallow sediment transport flow computation using time-varying sediment adaptation length. Int. J. Sediment Res. 29 (2), 171–183.
Quaresma, A., Pinheiro, A.N., 2021. Modelling of pool-type fishways flow: efficiency and scale effects assessment. Water 13, 852.
Ren, J., Wu, X., Zhang, T., 2021. A 3-D numerical simulation of the characteristics of open channel flows with submerged rigid vegetation. J. Hydrodyn. 33 (4), 833–843, 2021.
Rodi, W., 1993. Turbulence models and their application in hydraulics: a state-of-the art review. In: International Association for Hydraulic Research, third ed. A.A. Balkema, Rotterdam, Netherlands.
Ruonan, B., Liekai, C., Xingkui, W., Danxun, L., 2016. Comparison of ADV and PIV measurements in open channel flows. Procedia Eng. 154, 995–1001.
Smith, K.M., Caulfield, C.P., Taylor, J.R., 2021. Turbulence in forced stratified shear flows. J. Fluid Mech. 910, A42.
Solari, L., Van Oorschot, M., Belletti, B., et al., 2016. Advances on modelling riparian vegetation-hydromorphology interactions. River Res. Appl. 32, 164–178.
Spalart, P.R., 2000. Strategies for turbulence modelling and simulations. Int. J. Heat Fluid Flow 21 (3), 252–263.
Tariq, H., Ghani, U., Anjum, N., Pasha, G.A., 2022. 3D numerical modeling of flow characteristics in an open channel having in-line circular vegetation patches with varying density under submerged and emergent flow conditions. J. Hydrol. Hydromechanics 70 (1), 128–144.
Tasar, B., Unes, F., Gemici, E., Zelenakova, M., 2023. Experimental and numerical study on flow control using 3-array submerged vane in laboratory channel bend. Water 15 (4), 659.
Taylor, C.A., Figueroa, C.A., 2009. Patient-specific modeling of cardiovascular mechanics. Annu. Rev. Biomed. Eng. 11 (1), 109–134.
Taylor, C.A., Steinman, D.A., 2010. Image-based modelling of blood flow and vessel wall dynamics: applications, methods and future directions: Sixth International Bio-Fluid Mechanics Symposium and Workshop, March 28–30, 2008 Pasadena, California. Ann. Biomed. Eng. 38, 1188–1203.
Vijayasree, B.A., Eldho, T.I., Mazumder, B.S., 2020. Turbulence statistics of flow causing scour around circular and oblong piers. J. Hydraul. Res. 58 (4), 673–686.
Wang, P.-F., Wang, C., 2011. Numerical model for flow through submerged vegetation regions in a shallow lake. J. Hydrodyn. 23 (2), 170–178.
Xiang, K., Yang, Z., Huai, W., et al., 2019. Large eddy simulation of turbulent flow structure in a rectangular embayment zone with different population densities of vegetation. Environ. Sci. Pollut. Control Ser. 26, 14583–14597.
Xuecheng, F., Wang, F., Mengyang, L., Wenxin, H., 2020. Analysis of turbulent flow structures in the straight rectangular open channel with floating vegetated islands. Environ. Sci. Pollut. Control Ser. 27 (21), 26856–26867. https://doi.org/10.1007/s11356-020-09087-3.
Yakhot, V., Orszag, S., Thangam, S., Gatski, T., Speziale, C., 1992. Development of turbulence models for shear flows by a double expansion technique. Phys. Fluid. Fluid Dynam. 4 (7), 1510–1520. AIP Publ.
Zaffar, M.W., Hassan, I., 2023. Numerical investigation of hydraulic jump for different stilling basins using FLOW-3D. AQUA — Water Infrastructure, Ecosystems and Society 72 (7), 1320–1343.